Membranes with Highly Ordered Straight Nanopores by Selective Swelling of Fast Perpendicularly Aligned Block Copolymers

Jun Yin,[†,§] Xueping Yao,[†,§] Jiun-You Liou,[‡] Wei Sun,[†] Ya-Sen Sun,[‡] and Yong Wang[†,*]

[†]State Key Laboratory of Materials-Oriented Chemical Engineering, College of Chemistry and Chemical Engineering, Nanjing University of Technology, Nanjing, 210009 Jiangsu, China and [‡]Department of Chemical and Materials Engineering, National Central University, Taoyuan, 32001 Taiwan. [§]J.Y. and X.Y. contributed equally.

ABSTRACT Membranes with uniform, straight nanopores have important applications in diverse fields, but their application is limited by the lack of efficient producing methods with high controllability. In this work, we reported on an extremely simple and efficient strategy to produce such well-defined membranes. We demonstrated that neutral solvents were capable of annealing amphiphilic block copolymer (BCP) films of polystyrene-*block*-poly(2-vinylpyridine) (PS-*b*-P2VP) with thicknesses up to 600 nm to the perpendicular orientation within 1 min. Annealing in neutral solvents was also effective to the perpendicular alignment of block copolymers with very high molecular weights, *e.g.*, 362 000 Da. Remarkably, simply by immersing the annealed BCP films in hot ethanol followed by drying in air, the originally dense BCP films were nondestructively converted into porous membranes containing highly ordered, straight nanopores traversing the entire thickness of the membrane (up to 1.1 μm). Grazing incident small-angle X-ray spectroscopy confirmed the hexagonal ordering of the nanopores over large areas. We found that the overflow of P2VP chains from their reservoir P2VP cylinders and the deformation of the PS matrix in the swelling process contributed to the transformation of the solid P2VP cylinders to empty straight pores. The pore diameters can be tuned by either changing the swelling temperatures or depositing thin layers of metal oxides on the preformed membranes *via* atomic layer deposition with a subnanometer accuracy. To demonstrate the application of the obtained porous membranes, we used them as templates and produced centimeter-scale arrays of aligned nanotubes of metal oxides with finely tunable wall thicknesses.

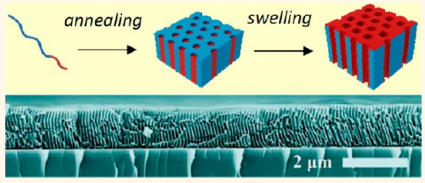

KEYWORDS: block copolymers · membranes · nanopores · solvent annealing · atomic layer deposition

Uniform straight pores with diameters below 50 nm provide confined spaces in which the transport, diffusion, and interactions of molecules may be qualitatively different than those in bulk spaces because of the confinement effect and interactions with the pore walls. A number of strategies, such as lithography,[1] anodization,[2] the use of aligned carbon nanotubes,[3,4] and the self-assembly of block copolymers (BCPs),[5,6] have been developed to fabricate porous membranes containing arrays of narrow and straight pores. Such membranes are finding important applications, such as in high-density storage media,[7,8] lithographic masks,[9] nanofluidics,[10] DNA sequencing,[11] advanced filters[12,13] and as templates for the synthesis of nanowires/rods.[14] Among the different methods to produce membranes with straight nanopores, the BCP route is distinctive for its effectiveness and flexibility, as it begins with BCP solutions and is capable of producing large-area membranes on substrates with different chemical properties and physical structures at low costs.[15,16] Block copolymers composed of two or more immiscible homopolymer chains covalently linked together tend to phase separate and will yield, under proper thermodynamic conditions, a variety of well-defined periodical structures with feature sizes typically falling in the range of 10−100 nm.[17−19] To create straight pores in BCPs, two critical steps are involved: (1) perpendicular alignment of the cylindrical phases in the BCP matrix and (2) removal of the aligned cylinders to yield straight pores. A number of external-fields-based methods have been developed to perpendicularly align the cylinders,[20−25] of which solvent annealing has been proved to be the easiest and most versatile.[26−30]

The solvent annealing method is based on the enhanced chain mobility obtained

* Address correspondence to yongwang@njut.edu.cn.

Received for review July 24, 2013 and accepted October 16, 2013.

Published online October 16, 2013
10.1021/nn403847z

when BCPs are exposed to the solvents that plasticize the polymer and significantly reduce the glass transition temperature (T_g). A number of BCPs have been perpendicularly aligned by annealing in various types of solvents. However, in many cases, this solvent annealing method is only applicable to thin BCP films with a thickness typically less than 100 nm. Both neutral solvents and selective solvents with preferential affinity only to one block have been used to induce the perpendicular alignment of the cylinders.[31,32] By comparison, neutral solvents may be more effective than selective ones for aligning block polymer films by solvent annealing if constituted blocks have high T_g's. The reason is that selective solvents only sufficiently swell one block. Because the other block lacks adequate mobility, a selective solvent may require longer periods of annealing time, *e.g.*, several hours, compared to a neutral solvent, to obtain a well-defined perpendicular orientation. Moreover, a selective solvent typically needs even longer annealing time to align BCPs with very high molecular weights,[33] limiting the tuning windows of structure parameters, including the cylinder diameters and spacings. Therefore, the highly controllable fast preparation of ordered, perpendicularly aligned BCP films with thicknesses greater than 100 nm remains a challenge. In terms of pore making, the aligned cylinders are usually converted into hollow pores using destructive methods, which are based on chemical etching of labile-blocks containing BCPs.[34−45] Unfortunately, destructive methods are only applicable to very limited types of BCPs, and frequently require harsh reaction conditions, such as UV-irradiation, alkali, ozone, or hydrofluoric acid (HF) to break the junction bonds between the constituent blocks. Moreover, a tedious pretreatment procedure involving rinsing and drying is typically involved. A nondestructive pore-making method is important because it provides the possibility to recycle the BCP starting materials for repeated uses. Surface reconstruction by immersing BCP thin films in solvents that selectively swell the minor component at ambient temperature has been effective for fabricating porous thin films of thickness less than 50 nm in a nondestructive way.[30,46,47]

In this work, we report on the extremely simple and efficient fabrication of membranes with highly ordered, straight nanopores by fast alignment of perpendicular cylinders in thick BCP films and the subsequent nondestructive transformation of the aligned cylinders into uniform straight pores. Amphiphilic block copolymers of cylinder-forming polystyrene-*block*-poly(2-vinylpyridine) (PS-*b*-P2VP) films with thicknesses up to 600 nm were perpendicularly aligned by a short annealing in chloroform which is a good solvent to both blocks for typically less than 1 min. This perpendicular alignment by annealing in neutral solvents is also effective for BCPs with very high molecular weights, *e.g.*, 362 000 Da. Remarkably, simply by immersing the annealed BCP films in hot ethanol followed by drying in air, the originally dense BCP films of submicrometer thickness were nondestructively converted into porous membranes containing highly ordered, straight nanopores traversing the entire thickness of the membrane. Another advantage of implementing immersion of BCP films in ethanol at elevated temperatures is that nanoporous thick membranes with tunable pore size can be tailored. We further demonstrated that the obtained BCP membranes can be used as templates to produce large-area arrays of aligned titanium oxide or aluminum oxide nanotubes by atomic layer deposition (ALD).

RESULTS

Fast Achievement of Perpendicular Alignment of PS-*b*-P2VP Films by Solvent Annealing. Cylinder-forming PS_{50k}-*b*-$P2VP_{16.5k}$ with 50 000- and 16 500-Da PS and P2VP blocks, respectively, was spin-coated on silicon substrates from its chloroform solution, producing films with a thickness of ~110−600 nm depending on the concentration of the solutions. The BCP films were subjected to annealing in the saturated vapor of chloroform operated in a glass chamber. We found that annealing for approximately 40 s at room temperature followed by instant evaporation of the solvent yielded a highly ordered perpendicular morphology. Figure 1 displays the morphology of a BCP film with a thickness of ~300 nm annealed in chloroform for 40 s. The scanning electron microscopy (SEM) image shown in Figure 1a reveals the annealed film possesses a dense, nonporous morphology with shallow concaves regularly patterned on the surface. The atomic force microscopy (AFM) height image (Figure 1b) confirms the presence of the shallow concaves with depth of approximately 2 nm hexagonally patterned on the surface, as schematically depicted in the inset in Figure 1a. The formation of this regularly concaved surface is due to the upper ends of the perpendicularly aligned P2VP cylinders being lower than the surrounding PS matrix, which is also observed in other annealed BCP films with perpendicular cylindrical morphology.[48] Inspired by our previous work in which P2VP cylinders randomly embedded in a PS matrix were converted into hollow pores when immersed in hot ethanol *via* the selective swelling-induced pore generation process,[49,50] we anticipated that P2VP phases embedded in the annealed BCP films may also be cavitated under appropriate swelling conditions. We immersed the annealed film in ethanol at 50 °C for 3 h, followed by air drying at room temperature, and examined the ethanol-treated film with SEM. As shown in Figure 1c, highly ordered circular pores appear on the surface of the ethanol-treated film. These pores are monodisperse, with a pore diameter of ~12 nm and are near-perfectly hexagonally arranged with an interpore distance of ~37 nm. More importantly, the cross-sectional SEM image (Figure 1d) indicates that these pores are

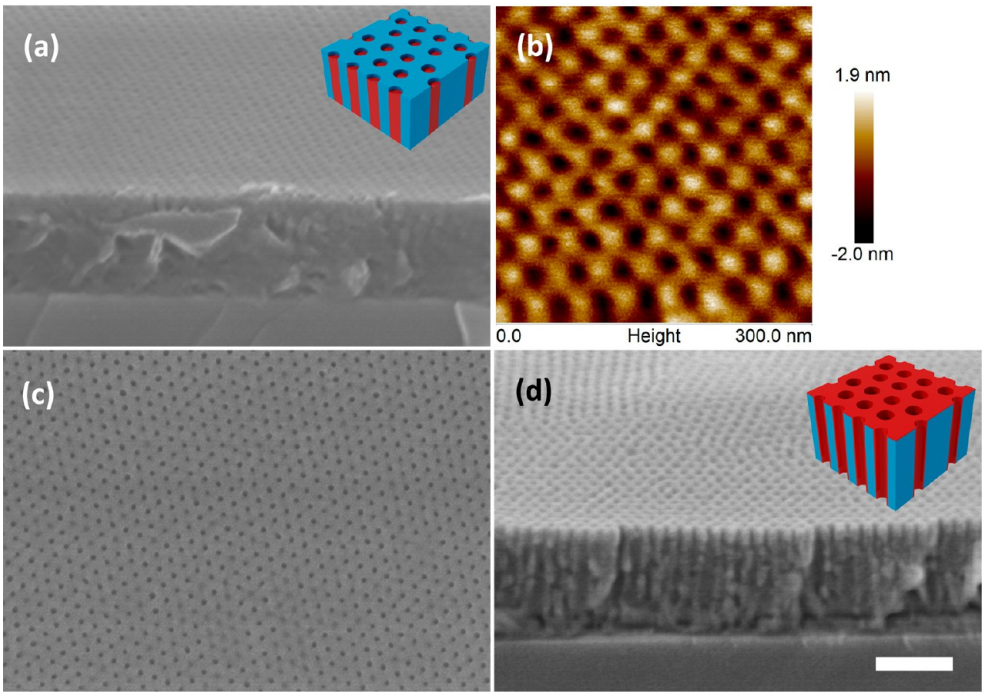

Figure 1. The 45°-tilted SEM image (a) and the 300 nm × 300 nm AFM height image (b) of PS_{50k}-*b*-$P2VP_{16.5k}$ films annealed in chloroform at room temperature for ~40 s. The top-view (c) and 45°-tilted (d) SEM images of the annealed film subjected to selective swelling in ethanol at 50 °C for 3 h, converting the P2VP cylinders into straight pores. Insets in (a) and (d) are the corresponding schematic structure of the annealed and ethanol-treated BCP films. PS and P2VP domains are highlighted in blue and red, respectively. (a), (c), and (d) have the same magnification. The scale bar is shown in (d) and corresponds to 200 nm.

straight, perpendicular to the film surface, and span the entire thickness of the film. Such a porous structure is schematically depicted in the inset in Figure 1d. The formation mechanism of the porous structure will be elucidated in the Discussion section. On the basis of the corresponding relationship between the pores and the P2VP microdomains in the BCP films before and after ethanol treatment, it is clear that annealing PS-*b*-P2VP films with a thickness of several hundreds of nanometers in chloroform vapor at room temperature for less than 1 min produces highly ordered P2VP cylinders perpendicularly aligned and spanning the entire thickness of the BCP film.

As electron microscopy only provides the ordering of the BCP membranes within very local areas, we used grazing incident small-angle X-ray spectroscopy (GISAXS) to characterize the structural details of the BCP films over several millimeters. As shown in Figure 2a, the 2D GISAXS pattern for the thin film annealed in chloroform only displays one symmetric set of principal Bragg diffraction-truncated rods. High-order Bragg rods were not present in the GISAXS pattern. In contrast, the GISAXS pattern for the film further subjected to immersion in ethanol displays a series of Bragg diffraction-truncated rods (Figure 2b). A comparison between the two patterns indicates that immersing BCP films in ethanol to create nanopores *via* selective swelling can increase the scattering intensity which is caused by the contrast of scattering length density between air and BCP films being larger than that between the PS and P2VP blocks. To improve the understanding of the in-plane structural information about the spatial order, we implemented a parallel scan cut to show the 1D scattering profiles (Figure 2c,d) As shown in Figure 2d, the in-plane 1D scattering profile for the BCP film with immersion in ethanol displays several sharp diffraction peaks at $q_{//}$ ratio $1:3^{1/2}:4^{1/2}:7^{1/2}:9^{1/2}:12^{1/2}$ with the first-order peak being at $q_{//} = 0.0185$ Å^{-1}. The q ratio indicates an in-plane two-dimensional hexagonal packing, and the peaks are associated to the (10), (11), (20), (21), (30), and (22) planes of the hexagon array. According to the position of the principal diffraction peak, the intercylinder distance is estimated to be ~39 nm, which is comparable to the intercylinder distance observed with SEM.

We examined the morphology of the PS_{50k}-*b*-$P2VP_{16.5k}$ film annealed in chloroform for different periods of time corresponding to different swelling degrees. The BCP film was sealed in the measuring chamber of an ellipsometer together with chloroform to monitor the thickness change of the film *in situ* during the solvent-annealing process. During annealing, the solvent molecules penetrated into the film and swollen the polymer chains, resulting in an increase in the film thickness. We withdrew the film from the chamber after annealing for a predetermined period of time, followed by immersion in hot ethanol to cavitate the P2VP phases for SEM observations. We found that the degree of swelling (D), denoted as the ratio of the thickness (d_t) of the swollen film to the initial thickness (d_0) of the BCP

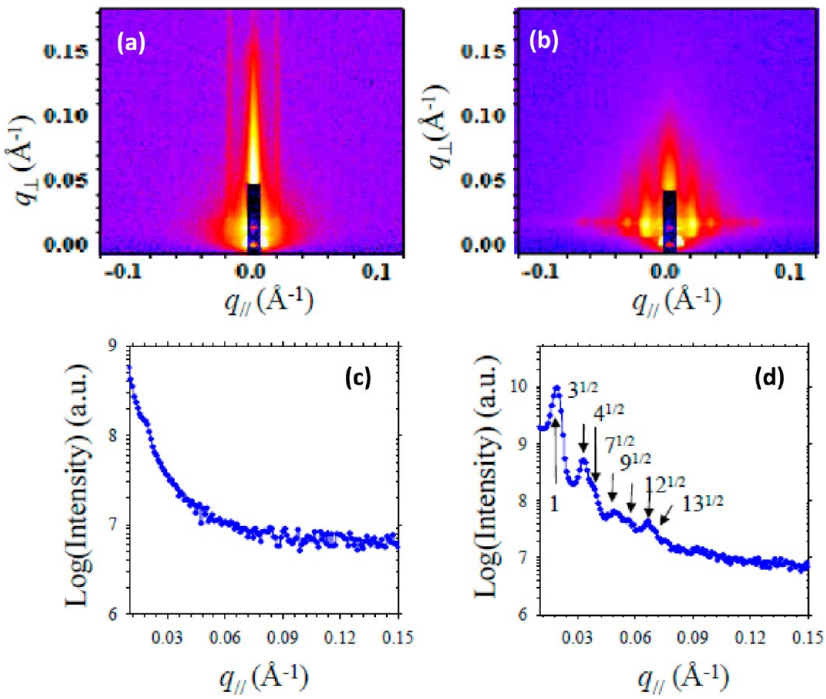

Figure 2. 2D GISAXS patterns and in-plane 1D scattering profiles of PS_{50k}-*b*-$P2VP_{16.5k}$ films annealed in chloroform at room temperature (a and c) and subsequently subjected to selective swelling in ethanol (b and d).

film before solvent annealing, significantly influenced the morphology of the annealed films. Figure 3 exhibits the morphology of BCP films annealed in chloroform with different *D* followed by ethanol treatment to transform the P2VP phases into pores. The initial thickness of the film before annealing is 110 nm and the film spin-coated on the Si substrate is blue. When the annealing film turned yellow at which $D = 1.57$, we withdrew the film from the annealing chamber, and the film immediately recovered to its original thickness and color because of the instant evaporation of chloroform. Figure 3a shows its morphology after ethanol treatment. We observed mainly circular pores corresponding to perpendicularly aligned P2VP cylinders in the film, but some channel-like pores were also present, indicating the coexistence of P2VP cylinders oriented parallel to the film surface. As the annealing proceeds, the swelling degree increases, resulting in films with more perpendicular P2VP cylinders than parallel ones (Figure 3b, $D = 1.7$). At $D = 1.89$, which is reached after annealing for 40 s, the swollen BCP turns reddish, and the film takes on the morphology of defect-free, hexagonally arranged perpendicular cylinders after evaporation of chloroform (Figure 3c). Further annealing leads to a continuous increase of *D* and a deterioration in the ordering of the film morphology, as shown in Figure 3d, where $D = 2.1$. The dependence of the annealed morphology on the swelling degree can be understood by the nucleation–growth mechanism dominating the perpendicular orientation of P2VP cylinders during solvent annealing.[51] At low swelling degrees, the mobility of polymer chains in the spin-coated BCP film is not adequate to trigger microphase separation. Nucleation of the ordered domains can not occur as the polymer chains are mainly in the frozen state.[52] Upon annealing the BCP films at moderate degrees of swelling in chloroform, the films might be in a homogeneous liquid (no microphase separated nanodmains exist) or have nanodomains with a much lower degree of ordering than the as-spun state. Regardless of the disordered states, quick drying creates a strong thermodynamic driving force to initiate and grow perpendicular cylinders with a lateral order of hexagonal lattice.[53] However, if the swelling ratio is too high, a few defects may be kinetically trapped within the films, further destroying the lateral order of perpendicular cylinders.

Perpendicular Alignment of BCPs with Very High Molecular Weights. The chain mobility decreases with increases in the molecular weight of BCP. Consequently, it is difficult to anneal BCPs with high molecular weights to yield well-defined phase-separated morphologies using a selective solvent as the annealing solvent. However, because neutral solvents have a strong affinity to both blocks, annealing in a neutral solvent should also be possible for BCPs with high molecular weights. We annealed films of PS_{290k}-*b*-$P2VP_{72k}$ with 290 000- and 72 500-Da PS and P2VP blocks, respectively, in chloroform at room temperature. As shown in Figure 4a, highly ordered, hexagonally arranged pores spanning the entire thickness of the film thickness after the annealing and the ethanol-swelling process are obtained, corresponding to a morphology of perpendicularly aligned P2VP cylinders. The corresponding GISAXS patterns further demonstrate that the high-molecular-weight

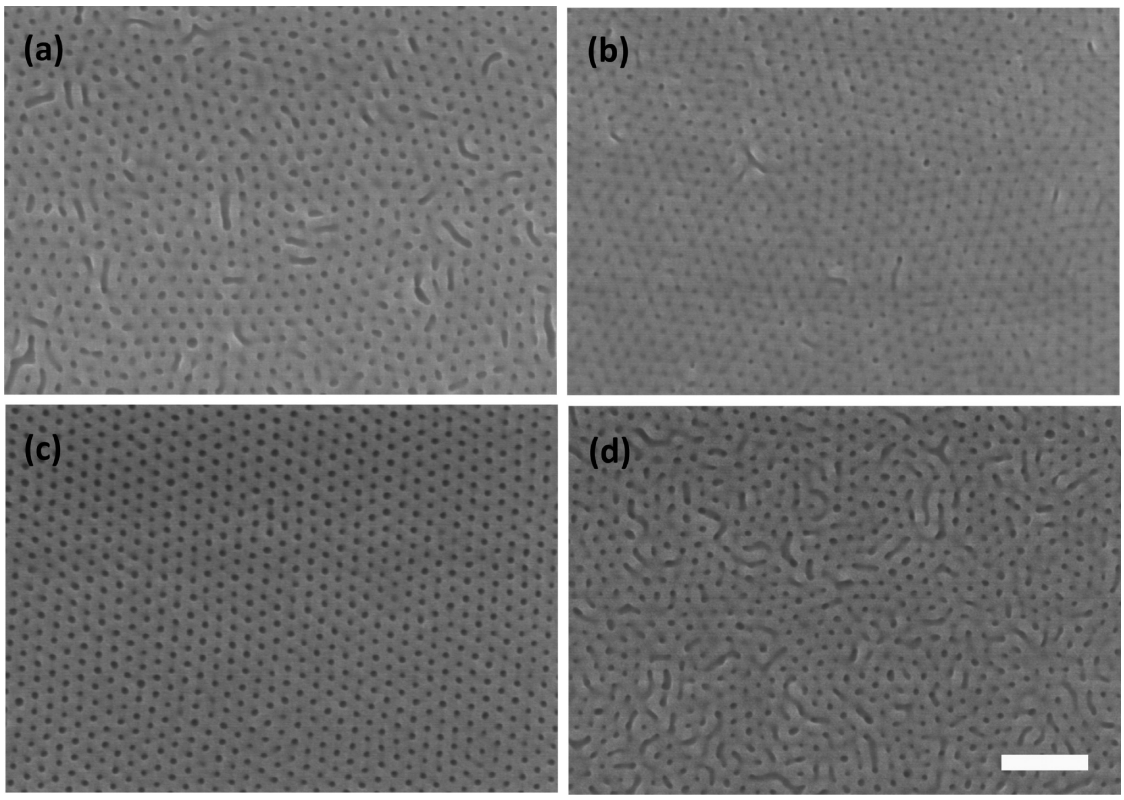

Figure 3. Top-view SEM images of PS_{50k}-*b*-$P2VP_{16.5k}$ films annealed in chloroform at room temperature for different swelling degrees: (a) 1.57, (b) 1.7, (c) 1.89, and (d) 2.1. All the annealed films were subjected to ethanol swelling to convert the P2VP phases to pores. (a–d) have the same magnification. The scale bar is shown in (d) and corresponds to 200 nm.

film reveals a series of Bragg diffraction rods, indicative of a high degree of spatial order (Figure S1). The pores have a diameter of ~46 nm and interpore spacing of ~91 nm, which are both noticeably larger than those of the porous membranes of PS-*b*-P2VP with smaller molecular weights, *e.g.*, PS_{50k}-*b*-$P2VP_{16.5k}$ (Figure 1). We note that BCPs with higher molecular weights require longer annealing times to reach the sufficiently solvated state for microphase separation. For instance, an annealing time of ~10 min is required for the film of PS_{290k}-*b*-$P2VP_{72k}$ to obtain a final perpendicular orientation of the P2VP cylinders whereas that for the PS_{50k}-*b*-$P2VP_{16.5k}$ film only requires 40 s. However, an annealing time of 10 min is still quite short compared to annealing times for selective solvents, which typically lasts for hours or days. Importantly, we found that PS_{290k}-*b*-$P2VP_{72k}$ films with a thickness up to 600 nm could also be perpendicularly aligned by annealing in chloroform followed by instant evaporation of chloroform. The formation of long P2VP cylinders perpendicular to the film surface should be attributed to three main factors: the strong immiscibility between PS and P2VP blocks as indicated by the large Flory–Huggins interaction parameter for PS and P2VP, $\chi_{PS\text{-}P2VP} = 47.0/T - 0.0176$,[54] the strong affinity of chloroform to both PS and P2VP blocks, and the low boiling point of chloroform (61.2 °C). The first two factors dictate that the nucleation of ordered phases occurred more at an earlier stage and the last one allows a stronger gradient in the solution concentration across the membrane thickness because of the quick evaporation of chloroform at room temperature, and consequently, a larger rate of the cylinder growth. Therefore, we were able to achieve the highly ordered perpendicular orientation of P2VP cylinders as high as 600 nm. The 600 nm-high P2VP cylinders are then converted into hollow pores with a height larger than 1.1 μm because of the significant increase in the film thickness during the selective swelling process (Figure 4b,c). Moreover, we measured the water contact angle (WCA) of the BCP film before and after chloroform annealing. The as-coated PS_{290k}-*b*-$P2VP_{72k}$ film exhibits a relatively high WCA of 90.5° which is close to that of the PS homopolymer. After annealing in chloroform, the WCA decreases to 82.7° indicating that the surface of the annealed film has been partially covered by the P2VP chains which are more hydrophilic compared to the PS chains. The ethanol-treated film displays a further reduced WCA of 74.7° which is similar to that of the P2VP homopolymer. Therefore, the upper ends of the perpendicular P2VP cylinders are directly exposed to free surface after the chloroform-annealing process while the film surface is completely covered by the P2VP chains overflew from the swollen P2VP cylinders. Compared to our previous work in which P2VP cylinders were randomly embedded in the nonannealed, as-coated film and completely surrounded by a PS matrix,[50] the exposed ends of P2VP cylinders in the chloroform-annealed film facilitate the diffusion of the

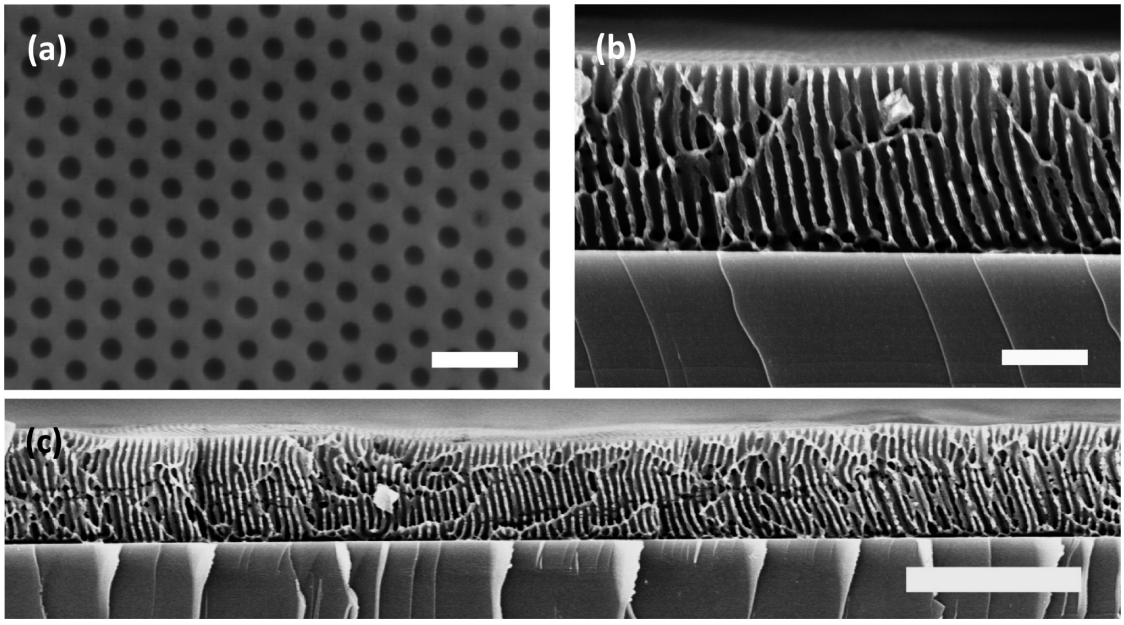

Figure 4. Top-view (a), cross-sectional (b and c) SEM images of PS_{290k}-*b*-$P2VP_{72k}$ films with a thickness of ~500 nm annealed in chloroform at room temperature for ~10 min, obtaining a perpendicular orientation for the P2VP cylinders. The annealed films were subjected to selective swelling in ethanol at 60 °C for 3 h, converting the P2VP cylinders into hollow channels. The scale bars shown in (a), (b), and (c) correspond to 200 nm, 500 nm, and 2 μm, respectively.

swelling agent into the interior of the P2VP cylinders because of the absence of a PS barrier layer. As a result, pore formation can be completed at a lower swelling temperature and/or within a shorter period of time.

Tuning the Diameters of the Straight Pores of the BCP Membranes. The pore diameters can be tuned using BCPs with different molecular weights, as demonstrated above. Moreover, some swelling parameters, such as swelling temperatures, can also be used to change the pore diameters. The swelling temperature dictates the mobility of the PS chains and the strength of the interaction of ethanol with P2VP chains, which both significantly influence the deformation degree of the PS matrix and correspondingly the pore sizes upon the collapse of the P2VP chains. Higher swelling temperatures lead to a stronger degree of both the deformation of the PS matrix and the overflow of P2VP chains and, consequently, larger pore diameters. As shown in Figure 5a–e, the pore diameters constantly increase as the swelling temperature increases from 40 to 70 °C. For example, the average pore diameter increases from ~18 nm at the swelling temperature of 40 °C to ~52 nm at the swelling temperature of 70 °C. The change in pore diameters with swelling temperature is quite sensitive: a 5 °C-increase in the swelling temperature typically enlarges the pore size by ~5 nm. However, the interpore distance remains almost unchanged with varying swelling temperatures (Figure 5f). Ever-increasing pore diameters and unchanged interpore distances imply that the pore walls (the PS matrix) are continuously thinned with increasing swelling temperatures because of the squeezing effect of the osmotic pressure accumulated in the P2VP cylinders. As a consequence of pore wall thinning, the membrane thickness increases to accommodate the squeezed PS chains. The swelling temperature significantly affects the increase of the thickness of the ethanol-treated films.

As clearly shown in Figure 5g, higher swelling temperatures result in greater increase in the film thickness. Swelling at temperatures below 50 °C gives rise to a <10% thickness increase. However, when the temperature is elevated to 55 °C, the thickness of the ethanol-treated film increases by 20%. Even higher swelling temperatures lead to correspondingly greater increases in thickness, for example, 80% at 70 °C. The correlation between swelling temperature and film thickness can easily be understood by the enhanced chain mobility of the PS matrix under higher temperatures, which leads to greater deformation degrees of the PS matrix in ethanol. Because of the confinement effect of the substrate surface, the BCP film could not change its lateral area along the substrate surface. The thickness increase of the BCP film subjected to ethanol treatment should be mainly attributed to the formation of pores, whereas the migration and deposition of P2VP chains on the original membrane surface also contribute the increase in film thickness. The contribution of the migrated P2VP chains becomes more pronounced at higher temperatures. Moreover, we are able to estimate the porosity of the membrane produced at different swelling temperatures using a well-established equation for cylindrical pores which correlates the porosity (ε) and the pore radii (r):[55]

$$\varepsilon = \frac{n_p \pi r^2}{A_m} \quad (1)$$

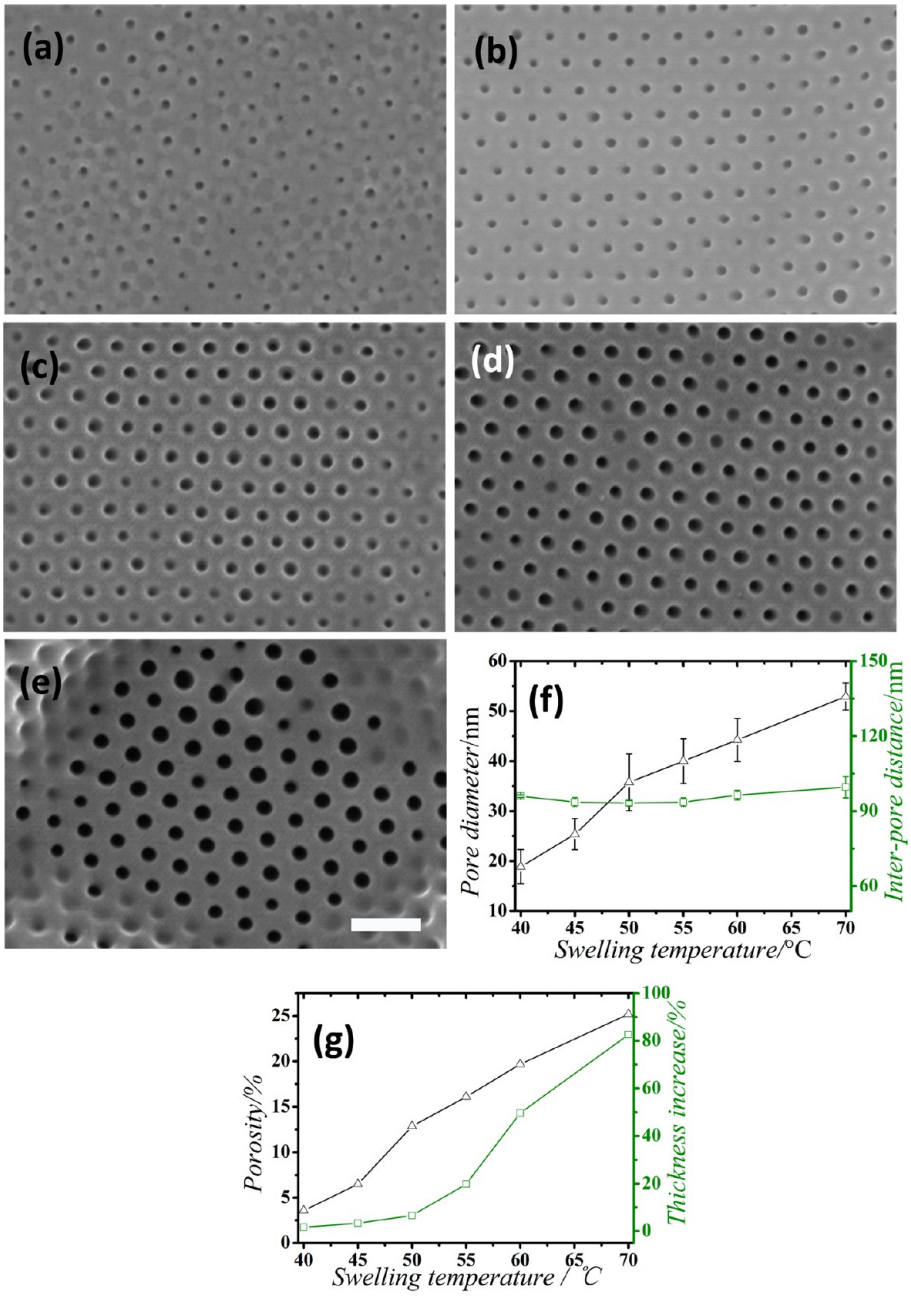

Figure 5. (a−e) Top-view SEM images of the chloroform-annealed PS_{290k}-*b*-$P2VP_{72k}$ films treated in ethanol for 3 h at different temperatures: (a) 40 °C, (b) 45 °C, (c) 50 °C, (d) 55 °C, and (e) 70 °C. The sample treated at 60 °C was depicted in Figure 4a. (f) Plots of the average pore diameter and the interpore distance as a function of swelling temperatures. (g) Plots of the percentage of thickness increase and porosity as a function of swelling temperatures. (a−e) have the same magnification. The scale bar in (e) corresponds to 200 nm.

where n_p is the number of pores and A_m is the external membrane area. As shown in Figure 5g, the porosities increase with the swelling temperatures. At a swelling temperature of 70 °C, the porosity is larger than 25% which is relatively high compared to other porous materials with hexagonally packed pores typically having a porosity of ~10%.[56] We note that the swelling temperature should be kept below the effective T_g of the PS block to hold the infrastructure of the porous membrane. As shown in Figure S2, swelling in ethanol at 75 °C for 3 h leads to partial detachment of the membrane from the substrate and morphology disordering in the detached regions. We also investigated the change of pore diameters with the periods of swelling time and found that the pore diameters were not sensitive to periods of swelling time. A short swelling for only 1 min is capable to yield pores with a diameter not significantly smaller than that of membrane being swollen for 5 h (Figure S3). This insensitive dependence of pore diameters on swelling time is because the exposed ends of P2VP cylinders have instant contact with ethanol upon immersion and the

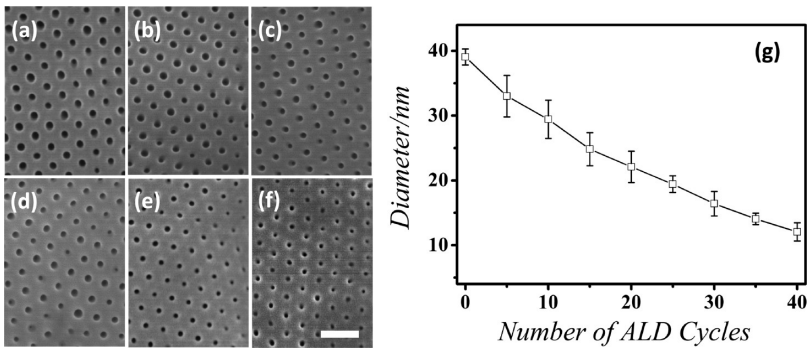

Figure 6. Top-view SEM images of porous membranes of PS_{290k}-*b*-$P2VP_{72k}$ subjected to 5 (a), 10 (b), 15 (c), 20 (d), 30 (e), and 40 (f) ALD cycles of Al_2O_3. (g) Plot of the average pore diameter as a function of the number of ALD cycles. (a–f) have the same magnification. The scale bar is shown in (f) and corresponds to 200 nm.

fast diffusion of ethanol into the interior of the P2VP cylinders at elevated temperatures.

In addition to tuning the pore size by changing the swelling temperatures during the membrane formation process, it would be very useful if one could modulate the pore size of preformed porous membranes using external methods. To this end, we deposited thin layers of Al_2O_3 on the BCP membranes using ALD. ALD is capable of producing conformal coatings on the surface of narrow pores as it is based on gas–solid reactions with a self-limiting nature. The swelling-induced porous membranes possessed active surfaces and pore walls covered by P2VP chains. Vaporized ALD precursors (TMA and water) can diffuse into the membrane pores and adsorb and react on the pore walls, producing a uniform coating of Al_2O_3 with a highly controllable thickness along the pore walls. As shown in Figure 6, the Al_2O_3-deposited membranes all exhibit a smooth surface because of the conformal growth of Al_2O_3 on the P2VP-covered surfaces. In addition, the uniformity of the pore size for the membranes subjected to different ALD cycles is maintained. Moreover, there is an almost linear decrease in pore size with increasing ALD cycle number. For example, the pore size of the 10-cycle-deposited membrane decreases from ~38 nm for the initial, nondeposited membrane to ~29 nm after 10 cycles of deposition and further decreases to ~15 nm after 40 cycles of deposition. Therefore, we can estimate that each ALD cycle produces a 0.6-nm-thick layer of Al_2O_3, which means that we can precisely and predictably tune the pore size using ALD with a subnanometer accuracy.

Fabrication of Nanotube Arrays from the Porous BCP Membranes. The obtained porous membranes possessed highly ordered pores with monodisperse pore sizes and a P2VP-covered, active pore surface.[57] Such membranes are expected to have interesting applications in diverse fields, including separation, drug delivery, lithography, and template synthesis. To demonstrate their potential applications, we used the obtained porous membranes as templates to synthesize centimeter-scale arrays of aligned metal oxides including TiO_2 and Al_2O_3 using ALD. As shown in Figure 7 and Figure S4, calcining the deposited membranes in air removes the BCP templates, producing aligned nanotubes connected at one end of the tubes by a surface layer. The hollow interiors of the nanotubes are discernible from the broken parts. Besides, there are some adjacent tubes interconnected at their bottom ends, forming U- or Y-shaped structures. Such interconnected structures were also observed in replicas produced from other block copolymer templates with cylindrical pores.[58] The presence of these structures implies that P2VP cylinders in the annealed BCP film are not always perfectly perpendicular near the substrate interface possibly because of the preferential affinity of P2VP chains to the hydrophilic surface of the Si surface. Because of the self-limiting nature of ALD reactions occurring in the vapor phase, deposition occurs along the pore walls inside the pores, producing a tube-like structure by replicating the contour of the pores. During the swelling process, the P2VP chains overflow onto the membrane surface and, following ALD also occurs on the membrane surface in addition to the pore interiors. Moreover, the thickness of the tube wall can be continuously tuned by changing the ALD cycle numbers (Figure S4). Considering that many materials, including oxides, metals, nitrides, and even polymers can be deposited on the templates of porous membranes using similar ALD protocols, we believe such a hierarchical structure of connected arrays of nanotubes will find interesting applications in the fields of control release, field emission devices, solar cells, *etc*.

DISCUSSION

Key Role of a Neutral Annealing Solvent in the Fast Perpendicular Alignment of BCP Films. Solvent selectivity, which means the difference of the affinity of the solvent to the constituent blocks of BCPs, plays a significant role in determining the orientation of BCP films after the annealing process. The polymer–solvent interaction parameter, $\chi_{polymer-solvent}$, reflects the affinity of a

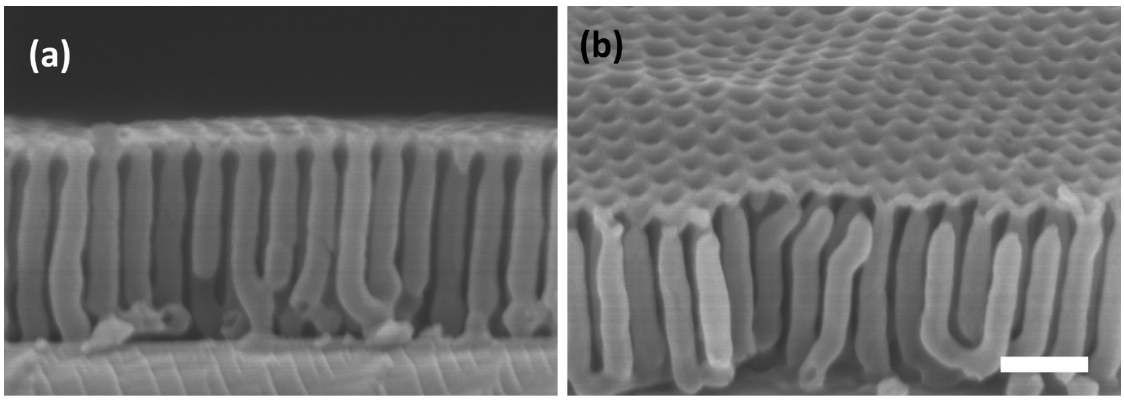

Figure 7. The cross-sectional (a) and 45°-tilted (b) SEM image of arrays of aligned TiO_2 nanotubes by ALD on porous membranes of PS_{290k}-*b*-$P2VP_{72k}$ with 200 ALD cycles. (a) and (b) have the same magnification and the scale bar shown in (b) corresponds to 200 nm.

TABLE 1. The polymer-solvent interaction parameters, molar volumes of solvents, and the solubility parameters of solvents and polymers involved in this work.[60]

solvent	molar volume/cm^3 mol^{-1}	$\delta_{solvent}$ /$(MPa)^{1/2}$	$\chi_{PS\text{-}solvent}$ (at 25 °C)	$\chi_{P2VP\text{-}solvent}$ (at 25 °C)	$\chi_{P4VP\text{-}solvent}$ (at 25 °C)
Chloroform	80.7	19	0.35	0.42	0.67

solvent to a polymer chain, which can be calculated using the following equation:[59]

$$\chi_{polymer\ -\ solvent} = V_{solvent}(\delta_{solvent} - \delta_{polymer})^2/RT + 0.34 \quad (2)$$

where $V_{solvent}$, $\delta_{solvent}$, $\delta_{polymer}$, R, and T are the molar volume of the solvent, the solubility parameter of the solvent and the polymer, gas constant (R = 8.314 J/(K·mol)), and the temperature in Kelvin, respectively. A lower value of $\chi_{polymer-solvent}$ means a better affinity of the solvent to the polymer. When $\chi_{polymer-solvent}$ is less than 0.5, the solvent is considered to be a good solvent for the polymer.[59] Table 1 summarizes the values of $\chi_{polymer-solvent}$ for different pairs of solvents and polymers involved in this work. As both $\chi_{PS\text{-chloroform}}$ and $\chi_{P2VP\text{-chloroform}}$ are less than 0.5 and they are close to each other, chloroform is considered to be a good solvent for both the PS block and the P2VP block. Therefore, chloroform is a neutral solvent for PS-*b*-P2VP. When chloroform is used as the solvent to anneal films of PS-*b*-P2VP, chloroform molecules quickly penetrate into both the PS and P2VP microdomains, strongly enhancing the mobility of both blocks. Because of the screening effect of the solvent molecules, the effective Flory–Huggins interaction parameter (χ_{eff}) between P2VP and PS decreases as the volume fraction (f_s) of the solvent in the film increases. Consequently, solvent uptake in the BCP films decreases the effective segregation strength, $\chi_{eff}N$, where N is the degree of polymerization. When annealed in a neutral solvent, the volume fraction of the solvent increased very rapidly because of the penetration of the solvent into both PS and P2VP phases. Consequently, $\chi_{eff}N$ decreased quickly, allowing the BCP film to gain adequate mobility for the onset of microphase separation within a very short time. This is the reason why a near-perfect perpendicular alignment could be achieved after an annealing time of less than 1 min using chloroform as the annealing solvent. At the end of solvent annealing, the annealing chamber was uncovered and the solvent was instantly evaporated from the BCP film.

To confirm the effect of the selectivity of the annealing solvent on the annealed morphology, we also annealed PS_{23k}-*b*-$P4VP_{4.5k}$ films with chloroform. The chloroform-annealed PS-*b*-P4VP film takes on a morphology of cylinders parallel to the film surface (Figure 8a), which is in stark contrast to that of PS-*b*-P2VP film annealed in the same solvent. This difference is caused by the greater affinity of chloroform to P2VP than to P4VP as evidenced by a larger value of $\chi_{P4VP\text{-chloroform}}$ than that of $\chi_{P2VP\text{-chloroform}}$ (Table 1). Moreover, we experimentally found that the dissolution of P4VP homopolymers in chloroform was slower than that of P2VP homopolymers, implying that chloroform is a weaker solvent for P4VP than P2VP. Therefore, chloroform is actually a somewhat selective solvent for PS-*b*-P4VP and annealing of PS-*b*-P4VP in chloroform gives rise to in-plane parallel cylinders. We added ethanol, which is a good solvent for P4VP, to chloroform to make it neutral to PS-*b*-P4VP and used the mixture to anneal PS_{23k}-*b*-$P4VP_{4.5k}$ films. We obtained highly ordered perpendicular cylinders as implied by the hexagonally arranged pores spanning the entire thickness of the film using the mixture of chloroform and ethanol (volume ratio = 10:1) as the annealing solvent (Figure 8b,c), which confirmed our conclusion that annealing in neutral solvents led to the perpendicular orientation of cylinders. We note that the morphology ordering of the PS-*b*-P4VP films annealed in different

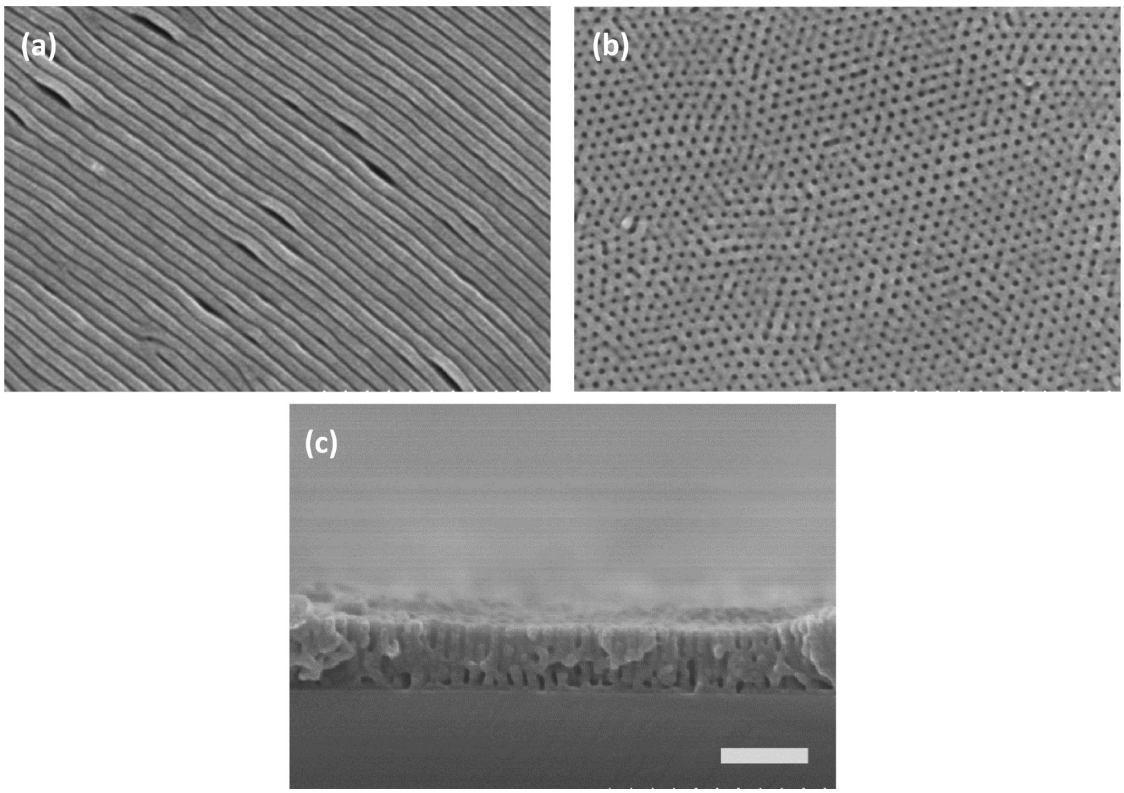

Figure 8. To-view surface images of PS_{23k}-*b*-$P4VP_{4.5k}$ films annealed in pure chloroform (a) and 10:1 (v/v) chloroform/ethanol (b). (c) The corresponding cross-sectional view SEM image of (b). All the annealed films were subjected to ethanol swelling to convert the P2VP cylinders to pores. (a−c) have the same magnification. The scale bar is shown in (c) and corresponds to 200 nm.

solvents is also dependent on *D*. Typically, the ordering of the annealed PS-*b*-P4VP film first increased with the rising of *D* and then deteriorated with further increased *D* after the highest ordering was achieved. For every sample, only the morphology with the highest ordering achieved in the entire investigated range of *D* was shown.

Formation Mechanism of Straight Pores inside the Annealed BCP Films. The formation of straight pores of the annealed BCP films upon ethanol treatment generally follows the selective swelling-induced pore generation mechanism.[30,48] In this process, the hot ethanol delivers two functions: swelling the P2VP phase and plasticizing the PS phase. When immersed in ethanol, the P2VP chains quickly take up ethanol, generating osmotic pressure inside the P2VP cylinders. The accumulated osmotic pressure drives the P2VP chains initially packed in the cylinders to overflow onto the film surface. Moreover, as the mobility of the PS chains is enhanced in hot ethanol, the osmotic pressure forces the PS framework to be stretched along the direction perpendicular to the film surface and compacted in the direction along the substrate surface. As a consequence, the volume of the P2VP cylinders expands. However, as the swelling temperature is controlled lower than the effective T_g of PS in ethanol, the structural integrity of the BCP film is maintained. With the evaporation of ethanol in the following air-drying procedure at room temperature, the streched PS matrix cannot recover to its initial state because the mobility of PS chains is reduced at room temperature, and the expanded spaces initially occupied by the solvated P2VP chains are frozen. However, the P2VP chains shrink and adopt a collapsed conformation with the loss of ethanol. Therefore, straight pores form in the positions occupied by the initial P2VP cylinders with the collapsed P2VP chains lined on the pore walls as they are chemically bonded to PS blocks. Scheme 1 displays a schematic description of the formation mechanism of straight pores in the annealed BCP films.

Such a mechanism of pore formation was confirmed by transmission electron microscopy (TEM). The chloroform-annealed PS_{290k}-*b*-$P2VP_{72k}$ films with a thickness of ~100 nm were transferred onto copper grids from their original Si substrates and then subjected to ethanol swelling. Figure 9a exhibits the TEM morphology of the annealed film prior to ethanol swelling. This film was stained with I_2 vapor and P2VP phases appeared darker because of the selective enrichment of I_2. Clearly, the TEM examination confirms the hexagonally packing of perpendicular P2VP cylinders in the PS matrix and the P2VP cylinders are presented as dark dots when viewed in the direction perpendicular to the film surface. As shown in Figure 9b, the ethanol-treated film

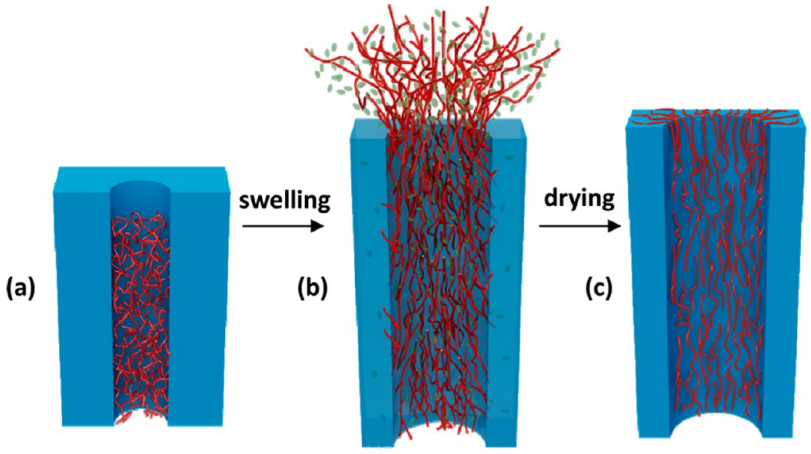

Scheme 1. Schematic description of the pore formation mechanism of the perpendicularly oriented PS-*b*-P2VP films treated in hot ethanol. (a) After solvent annealing, the P2VP chains (red) are condensed and packed as straight cylinders embedded in PS matrix (blue); (b) when immersed in hot ethanol (ellipsoids), the P2VP chains are swollen, leading to the overflow of the P2VP chains and the deformation of the PS matrix; (c) after drying in air, the P2VP chains collapsed on the membrane surface and pore walls, leading to the formation of straight pores in the positions of the initial P2VP cylinders

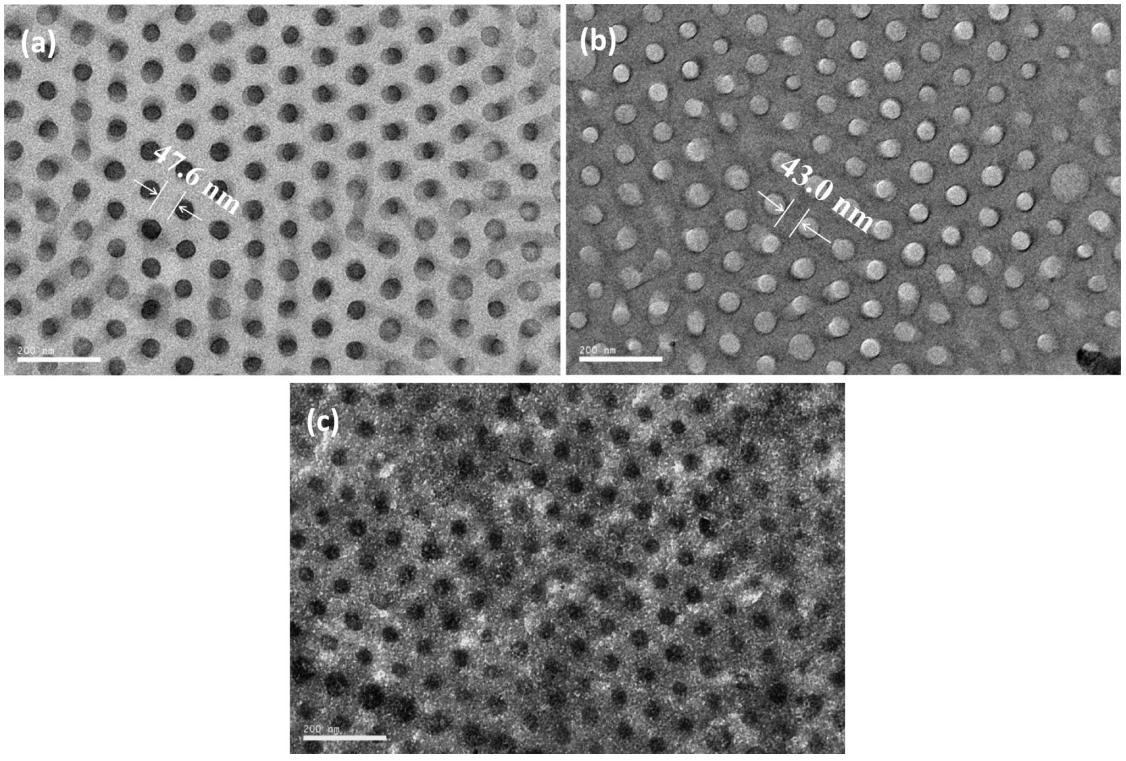

Figure 9. TEM images of chloroform-annealed PS_{290k}-*b*-$P2VP_{72k}$ films with a thickness of ~100 nm before (a) and after (b and c) treatment with ethanol at 60 °C for 3 h. The sample shown in (a) and (c) were stained with I_2 and the P2VP phases appeared darker than PS phases. The scale bars correspond to 200 nm. The average values of nearest distances of neighboring P2VP cylinders or pores are shown in the corresponding figures.

takes a porous morphology with pores maintaining the hexagonal arrangement of the initial P2VP cylinders. These pores can be easily discerned under TEM because they are in strong contrast with the surrounding polymeric matrix although the sample shown in Figure 9b is not stained. We further stained the ethanol-treated BCP film with I_2 to track the position of P2VP chains after the swelling process. As shown in Figure 9c, after staining with I_2 the pores are presented as dark rings and the regions between the pores/rings are also in the dark color, implying the presence of P2VP chains on the pore wall and the film surface. By comparing panels a and c of Figure 9, we confirm the overflow of P2VP chains on the film surface from the original P2VP cylinders during the ethanol swelling process (confirmed also by contact angle measurements described in the Results section).

Because of the covalent linkage of the P2VP blocks with the PS blocks, there is still a layer of P2VP chains

TABLE 2. Molecular Weights and Polydispersity Indexes (PDIs) of PS-*b*-P2VP and PS-*b*-P4VP Used in This Work

sample code	M_n of PS (kg/mol)	M_n of PVP (kg/mol)	PDI
PS_{50k}-*b*-$P2VP_{16.5k}$	50	16.5	1.09
PS_{290k}-*b*-$P2VP_{72k}$	290	72	1.10
PS_{23k}-*b*-$P4VP_{4.5k}$	23	4.5	1.10

tethering on the pore wall which is present as a dark ring under TEM after staining. Note that these dark rings show larger width than the real thickness of the P2VP layers lined on the pore wall because of the projection effect of the P2VP layers which do not always form an angle of exact 90° with the film surface. From Figure 9a, we determine that the average nearest distance of neighboring P2VP cylinders is 47.6 nm, whereas Figure 9b,c shows that the average nearest distance of neighboring pores is 43.0 nm. The reduced nearest distance after swelling reveals that the width of the PS wall between the pores becomes thinner in the *x* and *y* direction. As the BCP film is tightly fixed on the substrate surface, the compaction of the entire film on the substrate surface is not possible. Therefore, the thinning of the PS wall in the *x* and *y* direction is caused by the very local compaction of the PS wall driven by the swollen P2VP chains. As there is no weight loss during the swelling process, thinning of the PS wall in the *x* and *y* direction definitely leads to the increase of the height of the PS wall (also the film thickness) *via* the stretching of the PS chains in the *z* direction.

CONCLUSIONS

We demonstrated a very fast alignment of perpendicular cylinders in thick block copolymer films (*e.g.*, PS-*b*-P2VP) with thickness up to 600 nm by annealing in a neutral solvent which is a good solvent to both blocks for less than 1 min followed by instant evaporation of the solvent. Moreover, this annealing strategy is also effective to perpendicularly align BCPs with very high molecular weights (*e.g.*, 360 000 Da). Furthermore, highly ordered porous membranes with uniform straight nanopores spanning the entire thickness of the membrane were nondestructively obtained by an extremely simple selective swelling process. The osmotic pressure generated by the swelling P2VP chains in the P2VP cylinders, which were confined in the PS matrix, drove the overflow of the P2VP chains and the deformation of the PS matrix at elevated swelling temperatures. The P2VP cylinders were consequently transformed into straight pores lined with collapsed P2VP chains upon the evaporation of ethanol. The pore diameters of the nanopores were mainly determined by the molecular weights of BCPs and the swelling temperatures. Additionally, we showed that the pore size of the preformed porous BCP membranes could be continuously tuned by the deposition of thin layers of oxides by atomic layer deposition with a subnanometer accuracy. As a demonstration of the potential applications of the porous membranes, centimeter-scale arrays of aligned nanotubes of TiO_2 or Al_2O_3 were fabricated by atomic layer deposition on the porous membranes followed by calcination to remove the BCP membranes. The obtained porous membranes with uniform straight nanopores are expected to find interesting applications in various fields including separation, active coatings, drug delivery, and lithography.

METHODS

Materials. Three BCPs of poly(styrene-*block*-*x*-vinylpyridine) (PS-*b*-P*x*VP, $x = 2$ or 4) with various molecular weights were purchased from Polymer Source, Inc., and used as received. The compositional details of each BCP were listed in Table 2. All organic solvents including chloroform and ethanol, were of analytical grade and commercially acquired and used as received. Titanium tetrachloride ($TiCl_4$) with a purity of 99.99% was purchased from Aladdin Reagents. Trimethylaluminum (TMA) with a purity of >99.99% was obtained from Organometallics Center, Nanjing University. The block copolymers were dissolved in chloroform to obtain 1−3 wt % solutions. The polymer solutions were filtered 3 times through polytetrafluoroethylene (PTFE) filters with a nominal average pore size of 0.22 μm to remove any large aggregates. The BCP thin films were fabricated by spin-coating typically at 2000 rpm and 30 s, from its solution in chloroform on 1.5 cm × 1.5 cm silicon substrates.

Solvent Annealing. The BCP-deposited silicon substrates were transferred into a 70-mL weighing bottle which served as the annealing chamber filled with approximately 10 mL of the annealing solvent and placed on a support extending from the surface of the solvent inside the bottle. The bottle was covered with a lid immediately after placing the silicon substrates inside, allowing the annealing of the BCP films under saturated solvent vapor. The film changed color as the annealing proceeded. We investigated the morphology of the film with a thickness of 110 nm annealed in chloroform for different times. A highly ordered perpendicular morphology was reproducibly obtained when we terminated the annealing process at the point that the swollen 110-nm-thick film turned reddish by removing the lid of the chamber. In addition, we found that the thickness of BCP films did not influence the time required for the film to obtain the perpendicular orientation. It typically took ~40 s for the film to obtain a reddish color when annealing was carried out at 25 °C. To have a sensitive indicator of the perpendicular orientation, we always placed a 110-nm-film in the annealing chamber as a reference together with the film with a different thickness to be annealed in chloroform. When the reference turned reddish, we terminated the annealing process by opening the chamber to evaporate chloroform adsorbed in the film. To obtain porous membranes, the annealed BCP films were immersed in ethanol typically at 50 °C for 3 h unless otherwise stated to convert the P2VP or P4VP domains into pores.

ALD Deposition of Metal Oxides on Porous BCP Membranes. ALD deposition was carried out in a hot-wall ALD reactor (S-100, Cambridge) operated at 80 °C under a pressure of <1 Torr using N_2 as the carrier and purging gas. $TiCl_4$ and TMA were used as the metal precursor for the deposition of TiO_2 and Al_2O_3, respectively, while deionized water was used as the oxygen precursor in both cases. Vaporized precursors were alternatively pulsed into the ALD chamber, which was purged after the delivery of each precursor. We used the exposure mode of ALD to ensure sufficient precursor adsorption and penetration. For one growth cycle, the pulse and exposure times for both precursors were 0.015 and 20 s,

respectively. After each pulse of precursors, nitrogen purging lasting for 50 s was applied. To decompose the BCP templates, the deposited BCPs were heated to 540 °C at a heating rate of 9 °C/min in air and kept at this temperature for 4 h, then allowed to cool to room temperature.

Characterizations. The surface and cross-section morphologies of the samples were examined using a field emission scanning electron microscope (FESEM, Hitachi S4800) operated at 2 or 5 kV. The film thickness was measured by a spectroscopic ellipsometer (Complete EASE M-2000U, J. A. Woollam) with a 632.8 nm laser at a 75° incident angle. AFM images of the chloroform-annealed BCP films were obtained from an atomic force microscope in tapping mode (Bruker, MultiMode 8) equipped with silicon nitride cantilevers (Bruker TESPA, resonant frequency of 320 kHz). The structural information in reciprocal space was acquired by grazing incident small-angle X-ray scattering (GISAXS) measurements (Nano-Viewer, Rigaku). The parameters for operating Cu Kα X-rays of wavelength $\lambda = 1.54$ Å were 40 kV and 30 mA. The 2D GISAXS data were collected by PILATUS 100 K of 83.8 × 33.5 mm^2, in which an incident X-rays beam illuminated thin films at a grazing anlge of 0.1° or 0.2°. Each X-ray exposure duration lasted 20 min. The one-dimensional (1D) scattering intensity was clearly observed when in-plane scan cuts were imposed on the 2D GISAXS pattern to yield the 1D profile. Contact angles of droplets of deionized water on PS_{290k}-*b*-$P2VP_{72k}$ films subjected to different treatments were measured on five different positions of each sample by a contact angle goniometer (Dropmeter A-100, Maist) and the average value of the measurements was presented. To directly examine the morphology of the BCP film before and after swelling by TEM, we transferred the BCP films spincoated on silicon substrates onto copper grids. The solution of PS_{290k}-*b*-$P2VP_{72k}$ was spincoated on silicon substrates with a 1000-nm-thick SiO_x layer and then the BCP films, which had a thickness of ~100 nm, were annealed in chloroform to obtain a perpendicular orientation. We immersed the annealed BCP film supported on Si/SiO_x substrates in 5 wt % hydrofluoric acid to float the BCP film on the liquid surface by etching away the oxide layer between the BCP film and the silicon surface. The floating BCP film was collected on a copper grid and dried in air. The BCP film transferred on the copper grid was either stained with I_2 directly or first swelling treated in ethanol at 60 °C for 3 h to convert the P2VP cylinders into pores followed by I_2 staining. Staining was performed in a small glass chamber in which the samples were sealed together with I_2 crystals at 50 °C for 3 h. The BCP films transferred on copper grids, which were either stained or unstained, were probed with a JEOL 2100F TEM operating at 200 kV.

Conflict of Interest: The authors declare no competing financial interest.

Supporting Information Available: SEM images of porous BCP membranes prepared at different conditions, and aligned alumina nanotubes templated from porous membranes. GISAXS patterns of the perpendicularly aligned PS_{290k}-*b*-$P2VP_{72k}$ films before and after treatment in ethanol. This material is available free of charge *via* the Internet at http://pubs.acs.org.

Acknowledgment. Financial support from the Natural Science Foundation of China (21004033 and 21176120), the National Basic Research Program of China (2011CB612302), the Natural Science Research Program of the Jiangsu Higher Education Institutions (13KJA430005), the Jiangsu Natural Science Funds for Distinguished Young Scholars (BK2012039), and the Fok Ying Dong Education Foundation (131046) is gratefully acknowledged.

REFERENCES AND NOTES

1. Montagne, F.; Blondiaux, N.; Bojko, A.; Pugin, R. Molecular Transport through Nanoporous Silicon Nitride Membranes Produced from Self-Assembling Block Copolymers. *Nanoscale* **2012**, *4*, 5880–5886.
2. Masuda, H.; Fukuda, K. Oredered Metal Nanohole Arrays Made by a 2-Step Replication of Honeycomb Structures of Anodic Alumina. *Science* **1995**, *268*, 1466–1468.
3. Hinds, B. J.; Chopra, N.; Rantell, T.; Andrews, R.; Gavalas, V.; Bachas, L. G. Aligned Multiwalled Carbon Nanotube Membranes. *Science* **2004**, *303*, 62–65.
4. Holt, J. K.; Park, H. G.; Wang, Y. M.; Stadermann, M.; Artyukhin, A. B.; Grigoropoulos, C. P.; Noy, A.; Bakajin, O. Fast Mass Transport through Sub-2-Nanometer Carbon Nanotubes. *Science* **2006**, *312*, 1034–1037.
5. Morkved, T. L.; Lu, M.; Urbas, A. M.; Ehrichs, E. E.; Jaeger, H. M.; Mansky, P.; Russell, T. P. Local Control of Microdomain Orientation in Diblock Copolymer Thin Films with Electric Fields. *Science* **1996**, *273*, 931–933.
6. Tang, C.; Wu, W.; Smilgies, D. -M.; Matyjaszewski, K.; Kowalewski, T. Robust Control of Microdomain Orientation in Thin Films of Block Copolymers by Zone Casting. *J. Am. Chem. Soc.* **2011**, *133*, 11802–11809.
7. Park, S.; Lee, D. H.; Xu, J.; Kim, B.; Hong, S. W.; Jeong, U.; Xu, T.; Russell, T. P. Macroscopic 10-Terabit-per-Square-Inch Arrays from Block Copolymers with Lateral Order. *Science* **2009**, *323*, 1030–1033.
8. Thurn-Albrecht, T.; Schotter, J.; Kästle, G. A.; Emley, N.; Shibauchi, T.; Krusin-Elbaum, L.; Guarini, K.; Black, C. T.; Tuominen, M. T.; Russell, T. P. Ultrahigh-Density Nanowire Arrays Grown in Self-Assembled Diblock Copolymer Templates. *Science* **2000**, *290*, 2126–2129.
9. Tang, C.; Hur, S.; Stahl, B. C.; Sivanandan, K.; Dimitriou, M.; Pressly, E.; Fredrickson, G. H.; Kramer, E. J.; Hawker, C. J. Thin Film Morphology of Block Copolymer Blends with Tunable Supramolecular Interactions for Lithographic Applications. *Macromolecules* **2010**, *43*, 2880–2889.
10. Jiang, Y.; Liu, N.; Guo, W.; Xia, F.; Jiang, L. Highly-Efficient Gating of Solid-State Nanochannels by DNA Supersandwich Structure Containing ATP Aptamers: A Nanofluidic IMPLICATION Logic Device. *J. Am. Chem. Soc.* **2012**, *134*, 15395–15401.
11. Clarke, J.; Wu, H. C.; Jayasinghe, L.; Patel, A.; Reid, A.; Bayley, H. Continuous Base Identification for Single-Molecule Nanopore DNA Sequencing. *Nat. Nanotechnol.* **2009**, *4*, 265–270.
12. Yang, S. Y.; Ryu, I.; Kim, H. Y.; Kim, J. K.; Jang, S. K.; Russell, T. P. Nanoporous Membranes with Ultrahigh Selectivity and Flux for the Filtration of Viruses. *Adv. Mater.* **2006**, *18*, 709–712.
13. Xu, T.; Zhao, N.; Ren, F.; Hourani, R.; Lee, M. T.; Shu, J. Y.; Mao, S.; Helms, B. A. Subnanometer Porous Thin Films by the Co-assembly of Nanotube Subunits and Block Copolymers. *ACS Nano* **2011**, *5*, 1376–1384.
14. Lee, J. I.; Cho, S. H.; Park, S. -M.; Kim, J. K.; Kim, J. K.; Yu, J. -W.; Kim, Y. C.; Russell, T. P. Highly Aligned Ultrahigh Density Arrays of Conducting Polymer Nanorods Using Block Copolymer Templates. *Nano Lett.* **2008**, *8*, 2315–2320.
15. Hillmyer, M. Nanoporous Materials from Block Copolymer Precursors. *Adv. Polym. Sci.* **2005**, *190*, 137–181.
16. Olson, D. A.; Chen, L.; Hillmyer, M. A. Templating Nanoporous Polymers with Ordered Block Copolymers. *Chem. Mater.* **2008**, *20*, 869–890.
17. Bates, F. S.; Fredrickson, G. H. Block Copolymer Thermodynamics: Theory and Experiment. *Annu. Rev. Phys. Chem.* **1990**, *41*, 525–557.
18. Abetz, V.; Simon, P. F. W. Phase Behaviour and Morphologies of Block Copolymers. *Adv. Polym. Sci.* **2005**, *189*, 125–212.
19. Darling, S. B. Directing the Self-Assembly of Block Copolymers. *Prog. Polym. Sci.* **2007**, *32*, 1152–1204.
20. Mansky, P.; Russell, T. P.; Hawker, C. J.; Mays, J.; Cook, D. C.; Satija, S. K. Interfacial Segregation in Disordered Block Copolymers: Effect of Tunable Surface Potentials. *Phys. Rev. Lett.* **1997**, *79*, 237–240.
21. Huang, E.; Russell, T. P.; Harrison, C.; Chaikin, P. M.; Register, R. A.; Hawker, C. J.; Mays, J. Using Surface Active Random Copolymers To Control the Domain Orientation in Diblock Copolymer Thin Films. *Macromolecules* **1998**, *31*, 7641–7650.
22. Mansky, P.; Liu, Y.; Huang, E.; Russell, T. P.; Hawker, C. J. Controlling Polymer-Surface Interactions with Random Copolymer Brushes. *Science* **1997**, *275*, 1458–1460.

23. Han, E.; Stuen, K. O.; Leolukman, M.; Liu, C. -C.; Nealey, P. F.; Gopalan, P. Perpendicular Orientation of Domains in Cylinder-Forming Block Copolymer Thick Films by Controlled Interfacial Interactions. *Macromolecules* **2009**, *42*, 4896–4901.
24. Thurn-Albrecht, T.; DeRouchey, J.; Russell, T. P. Overcoming Interfacial Interactions with Electric Fields. *Macromolecules* **2000**, *33*, 3250–3253.
25. She, M. S.; Lo, T. Y.; Ho, R. M. Long-Range Ordering of Block Copolymer Cylinders Driven by Combining Thermal Annealing and Substrate Functionalization. *ACS Nano* **2013**, *7*, 2000–2011.
26. Sidorenko, A.; Tokarev, I.; Minko, S.; Stamm, M. Ordered Reactive Nanomembranes/Nanotemplates from Thin Films of Block Copolymer Supramolecular Assembly. *J. Am. Chem. Soc.* **2003**, *125*, 12211–12216.
27. Park, S.; Wang, J. -Y.; Kim, B.; Chen, W.; Russell, T. P. Solvent-Induced Transition from Micelles in Solution to Cylindrical Microdomains in Diblock Copolymer Thin Films. *Macromolecules* **2007**, *40*, 9059–9063.
28. Park, S.; Kim, B.; Xu, J.; Hofmann, T.; Ocko, B. M.; Russell, T. P. Lateral Ordering of Cylindrical Microdomains Under Solvent Vapor. *Macromolecules* **2009**, *42*, 1278–1284.
29. Kim, S. H.; Misner, M. J.; Xu, T.; Kimura, M.; Russell, T. P. Highly Oriented and Ordered Arrays from Block Copolymers *via* Solvent Evaporation. *Adv. Mater.* **2004**, *16*, 226–231.
30. Park, S.; Wang, J.-Y.; Kim, B.; Xu, J.; Russell, T. P. A Simple Route to Highly Oriented and Ordered Nanoporous Block Copolymer Templates. *ACS Nano* **2008**, *2*, 766–772.
31. Gowd, E. B.; Böhme, M.; Stamm, M. *In Situ* GISAXS Study on Solvent Vapour Induced Orientation Switching in PS-b-P4VP Block Copolymer Thin Films. *IOP Conf. Ser.: Mater. Sci. Eng.* **2010**, *14*, 012015/1–012015/6.
32. Phillip, W. A.; O'Neill, B.; Rodwogin, M.; Hillmyer, M. A.; Cussler, E. L. Self-Assembled Block Copolymer Thin Films as Water Filtration Membranes. *ACS Appl. Mater. Interfaces* **2010**, *2*, 847–853.
33. Kim, E.; Ahn, H.; Park, S.; Lee, H.; Lee, M.; Lee, S.; Kim, T.; Kwak, E. -A.; Lee, J. H.; Lei, X.; *et al.* Directed Assembly of High Molecular Weight Block Copolymers: Highly Ordered Line Patterns of Perpendicularly Oriented Lamellae with Large Periods. *ACS Nano* **2013**, *7*, 1952–1960.
34. Wang, Y.; Gösele, U.; Steinhart, M. Mesoporous Polymer Nanofibers by Infiltration of Block Copolymers with Sacrificial Domains into Porous Alumina. *Chem. Mater.* **2008**, *20*, 379–381.
35. Crossland, E. J. W.; Kamperman, M.; Nedelcu, M.; Ducati, C.; Wiesner, U.; Smilgies, D. M.; Toombes, G. E. S.; Hillmyer, M. A.; Ludwigs, S.; Steiner, U.; *et al.* A Bicontinuous Double Gyroid Hybrid Solar Cell. *Nano Lett.* **2009**, *9*, 2807–2812.
36. Crossland, E. J. W.; Nedelcu, M.; Ducati, C.; Ludwigs, S.; Hillmyer, M. A.; Steiner, U.; Snaith, H. J. Block Copolymer Morphologies in Dye-Sensitized Solar Cells: Probing the Photovoltaic Structure-Function Relation. *Nano Lett.* **2009**, *9*, 2813–2819.
37. Pitet, L. M.; Amendt, M. A.; Hillmyer, M. A. Nanoporous Linear Polyethylene from a Block Polymer Precursor. *J. Am. Chem. Soc.* **2010**, *132*, 8230–8231.
38. Tseng, Y. T.; Tseng, W. H.; Lin, C. H.; Ho, R. M. Fabrication of Double-Length-Scale Patterns *via* Lithography, Block Copolymer Templating, and Electrodeposition. *Adv. Mater.* **2007**, *19*, 3584–3588.
39. Hsueh, H. Y.; Chen, H. Y.; She, M. S.; Chen, C. K.; Ho, R. M.; Gwo, S.; Hasegawa, H.; Thomas, E. L. Inorganic Gyroid with Exceptionally Low Refractive Index from Block Copolymer Templating. *Nano Lett.* **2010**, *10*, 4994–5000.
40. Hsueh, H. Y.; Huang, Y. C.; Ho, R. M.; Lai, C. H.; Makida, T.; Hasegawa, H. Nanoporous Gyroid Nickel from Block Copolymer Templates *via* Electroless Plating. *Adv. Mater.* **2011**, *23*, 3041–3046.
41. Park, M.; Harrison, C.; Chaikin, P. M.; Register, R. A.; Adamson, D. H. Block Copolymer Lithography: Periodic Arrays of $\sim 10^{11}$ Holes in 1 Square Centimeter. *Science* **1997**, *276*, 1401–1404.
42. Hashimoto, T.; Tsutsumi, K.; Funaki, Y. Nanoprocessing Based on Bicontinuous Microdomains of Block Copolymers: Nanochannels Coated with Metals. *Langmuir* **1997**, *13*, 6869–6872.
43. Chan, V. Z. H.; Hoffman, J.; Lee, V. Y.; Iatrou, H.; Avgeropoulos, A.; Hadjichristidis, N.; Miller, R. D.; Thomas, E. L. Ordered Bicontinuous Nanoporous and Nanorelief Ceramic Films from Self Assembling Polymer Precursors. *Science* **1999**, *286*, 1716–1719.
44. Ndoni, S.; Vigild, M. E.; Berg, R. H. Nanoporous Materials with Spherical and Gyroid Cavities Created by Quantitative Etching of Polydimethylsiloxane in Polystyrene-Polydimethylsiloxane Block Copolymers. *J. Am. Chem. Soc.* **2003**, *125*, 13366–13367.
45. Li, L.; Schulte, L.; Clausen, L. D.; Hansen, K. M.; Jonsson, G. E.; Ndoni, S. Gyroid Nanoporous Membranes with Tunable Permeability. *ACS Nano* **2011**, *5*, 7754–7766.
46. Boontongkong, Y.; Cohen, R. E. Cavitated Block Copolymer Micellar Thin Films: Lateral Arrays of Open Nanoreactor. *Macromolecules* **2002**, *35*, 3647–3652.
47. Xu, T.; Stevens, J.; Villa, J. A.; Goldbach, J. T.; Guarini, K. W.; Black, C. T.; Hawker, C. J.; Russell, T. P. Block Copolymer Surface Reconstuction: A Reversible Route to Nanoporous Films. *Adv Func. Mater.* **2003**, *9*, 698–702.
48. Park, S.; Kim, B.; Wang, J. Y.; Russell, T. P. Fabrication of Highly Ordered Silicon Oxide Dots and Stripes from Block Copolymer Thin Films. *Adv. Mater.* **2008**, *20*, 681–685.
49. Wang, Y.; Li, F. B. An Emerging Pore-Making Strategy: Confined Swelling-Induced Pore Generation in Block Copolymer Materials. *Adv. Mater.* **2011**, *23*, 2134–2148.
50. Wang, Y.; He, C. C.; Xing, W. H.; Li, F. B.; Tong, L.; Chen, Z. Q.; Liao, X. Z.; Steinhart, M. Nanoporous Metal Membranes with Bicontinuous Morphology from Recyclable Block-Copolymer Templates. *Adv. Mater.* **2010**, *22*, 2068–2072.
51. Phillip, W. A.; Hillmyer, M. A.; Cussler, E. L. Cylinder Orientation Mechanism in Block Copolymer Thin Films upon Solvent Evaporation. *Macromolecules* **2010**, *43*, 7763–7770.
52. Paik, M. Y.; Bosworth, J. K.; Smilges, D. M.; Schwartz, E. L.; Andre, X.; Ober, C. K. Reversible Morphology Control in Block Copolymer Films *via* Solvent Vapor Processing: An *in Situ* GISAXS Study. *Macromolecules* **2010**, *43*, 4253–4260.
53. Kim, S. H.; Misner, M. J.; Xu, T.; Kimura, M.; Russell, T. P. Highly Oriented and Ordered Arrays from Block Copolymers *via* Solvent Evaporation. *Adv. Mater.* **2004**, *16*, 226–231.
54. Zha, W.; Han, C. D.; Lee, D. H.; Han, S. H.; Kim, J. K.; Kang, J. H.; Park, C. Origin of the Difference in Order−Disorder Transition Temperature between Polystyrene-Block-Poly(2-vinylpyridine) and Polystyrene-Block-Poly(4-vinylpyridine) Copolymers. *Macromolecules* **2007**, *40*, 2109–2119.
55. Hollman, A. M.; Bhattacharyya, D. Pore Assembled Multilayers of Charged Polypeptides in Microporous Membranes for Ion Separation. *Langmuir* **2004**, *20*, 5418–5424.
56. Nielsch, K.; Choi, J.; Schwirn, K.; Wehrspohn, R. B.; Gösele, U. Self-Ordering Regimes of Porous Alumina: The 10% Porosity Rule. *Nano Lett.* **2002**, *2*, 677–680.
57. Wang, Z. G.; Yao, X. P.; Wang, Y. Swelling-Induced Mesoporous Block Copolymer Membranes with Intrinsically Active Surfaces for Size-Selective Separation. *J. Mater. Chem.* **2012**, *22*, 20542–20548.
58. Vayer, M.; Nguyen, T. H.; Grosso, D.; Boissiere, C.; Hillmyer, M. A.; Sinturel, C. Characterization of Nanoporous Polystyrene Thin Films by Environmental Ellipsometric Porosimetry. *Macromolecules* **2011**, *44*, 8892–8897.
59. Huang, H.; Hu, Z.; Chen, Y.; Zhang, F.; Gong, Y.; He, T. Effects of Casting Solvents on the Formation of Inverted Phase in Block Copolymer Thin Films. *Macromolecules* **2004**, *37*, 6523–6530.
60. Brandrup, J.; Immergut, E. H.; Grulke, E. A.; Abe, A.; Bloch, D. R., Eds. *Polymer Handbook*, 4th ed.; John Wiley & Sons: New York, 1999; pp VII675−VII714.